Chinese Journal of Physics 57 (2019) 348–361

Contents lists available at ScienceDirect

Chinese Journal of Physics

journal homepage: www.elsevier.com/locate/cjph

Synthesis, experimental and theoretical analysis, and antiproliferative activity of 2-(4-methoxyphenylamino)-2-oxoethyl methacrylate

Emine Tanış[a,*], Nevin Çankaya[b], Serap Yalçın[c]

[a] Kırşehir Ahi Evran University, Kaman Vocational School, Kırsehir, Turkey
[b] Usak University, Department of Chemistry, Usak, Turkey
[c] Kırşehir Ahi Evran University, Department of Molecular Biology and Genetic, Kırsehir, Turkey

ARTICLE INFO

Keywords:
2-(4-methoxyphenylamino)-2-oxoethyl methacrylate (MPAEMA)
Density functional theory
Time-dependent approach
HeLa cell line
Antiproliferative activity

ABSTRACT

In this study 2-(4-methoxyphenylamino)-2-oxoethyl methacrylate (MPAEMA) has been synthesized and characterized experimentally (FTIR, NMR). Theoretically, physical, electronic and vibrational properties of MPAEMA molecule have been investigated using density functional theory (DFT) calculations at B3LYP/6-311 + + G(d,p) basis set. Bond distance, FTIR spectrum, NMR spectra and vibrational frequencies have been carried out. The calculated FTIR and NMR spectra of the headline molecule from the DFT have been compared with the measured ones, and good results have been obtained. UV spectrum characteristics and the electronic properties, like frontier orbitals, and band gap energy of MPAEMA have also been recorded by time-dependent (TD-DFT) method based on optimized structure with different solvent. The experimental results have been compared with theoretical values. Both experimental and theoretical methods have shown that the compound has successfully been synthesized. Cytotoxicity of MPAEMA has been investigated by XTT cell proliferation assay. IC50 values of MPAEMA have been identified as 1.8 mM on HeLa cell line.

1. Introduction

Acrylate and methacrylate derivatives are among the chemicals frequently used to enhance the functionality of the materials. One of the most important properties of methacrylate monomers is their optical transparency. Due to their high light transmittance, good mechanical and thermal durability, they have a wide range of applications [1]. Thanks to these physical properties; acrylates are used in medicine, orthopedics, tooth and filling materials, drug delivery systems, biochemical sensors and soft tissue studies [2–4]. Knowing the geometric, physical and chemical properties of monomeric molecules supported by theoretical methods is very important in terms of leading experimental studies. The values calculated with theoretical Density Functional Theory (DFT) and Hartree–Fock (HF) are very close to the experimental results [5]. In addition, the DFT method provides significant findings with low computational cost for organic molecules [6], organometallic compounds [7] and polymers [8].

As far as we are know, there have been no reports about the structural, electronic, spectroscopic and antitumor properties of MPAEMA molecule. In this work, 2-(4-methoxyphenylamino) − 2-oxoethyl methacrylate has been synthesized and characterized, both experimentally and theoretically, also the antiproliferative effects of the compound have been investigated on HeLa cancer cell

* Corresponding author.
E-mail address: eminetanis@ahievran.edu.tr (E. Tanış).

https://doi.org/10.1016/j.cjph.2018.11.006
Received 30 March 2018; Received in revised form 26 June 2018; Accepted 19 November 2018
Available online 22 November 2018

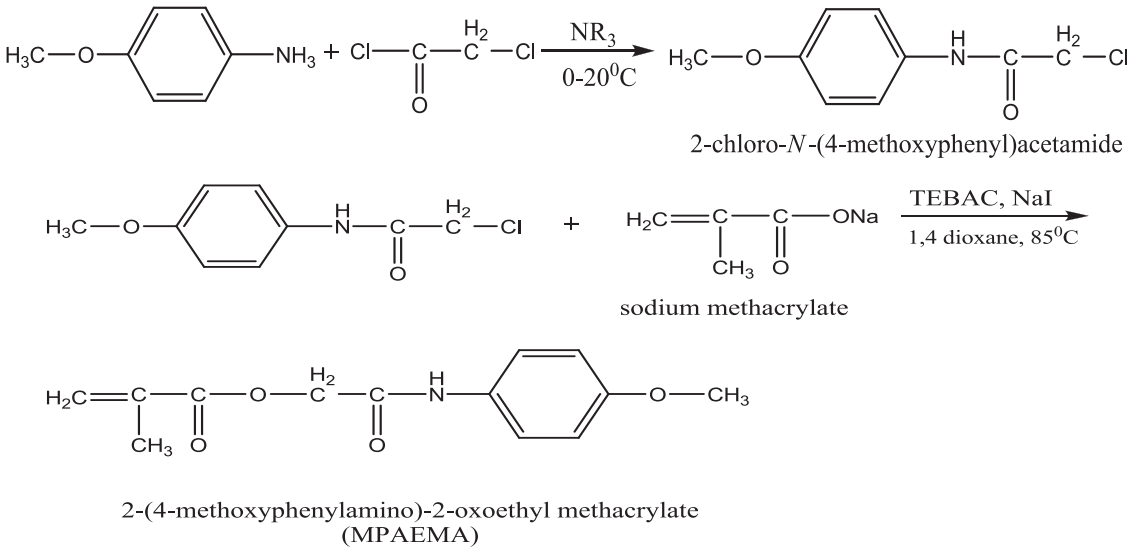

Fig. 1. The synthesis scheme of MPAEMA.

line.

2. Materials and methods

2.1. Synthesis of 2-(4-methoxyphenylamino) − 2-oxoethyl methacrylate (MPAEMA)

Chloroacetyl chloride, p-methoxyaniline, and triethylamine (NR_3) have been reacted while acetone has used as a solvent, yielding to 2-chloro-N-(4-methoxyphenyl) acetamide. 2-chloro-N-(4-methoxyphenyl) acetamide and sodium methacrylate have been reacted, while Tebac and NaI as phase transfer catalysts, 1,4-Dioxane as solvent, and refluxed meanwhile [9–11]. The yield has calculated as 83%. Synthesized MPAEMA is shown in Fig. 1.

2.2. Spectroscopy studies

Infrared spectrum has recorded in an A PerkinElmer Spectrum Two (UATR) IR spectrometer. The calculated optimized geometry of MPAEMA molecule has depicted in Fig. 2 along with their atomic numbers. The geometry of MPAEMA has been optimized by using Becke's three parameters hybrid density function at B3LYP/6-311 + + G(d,p) theoretical level, that includes both DFT exchange correlation and Hartree-Fock exchange functions [12–14]. All quantum chemical calculations has conducted by using the Gaussian 09 programs [15].

For conformational properties and flexibility, the molecular energy profile has been obtained with a rotation from 0° to 360° in every 10° at the selected torsional freedom degrees of T (C23-C22-O29-C30) and T(O11-C9-C8-C1) (Fig. 3). Theoretical results have

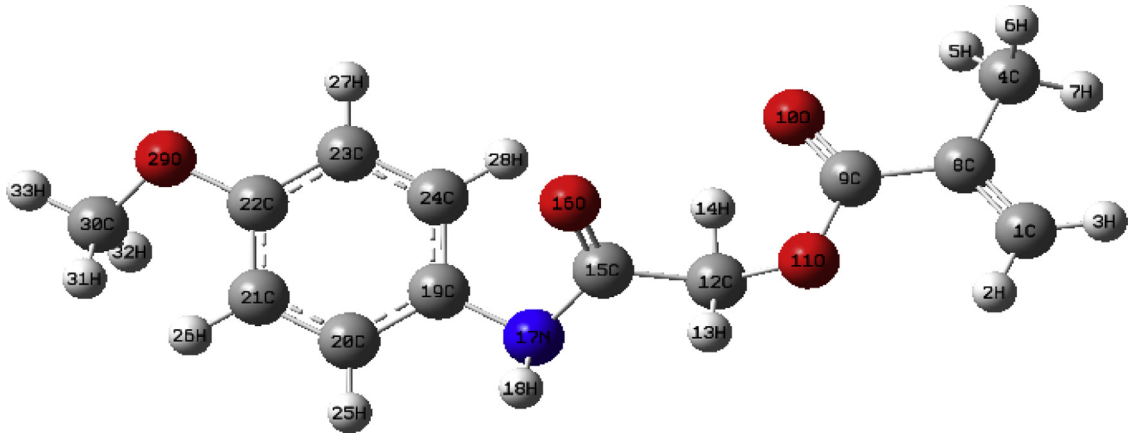

Fig. 2. The theoretical geometric structures of MPAEMA.

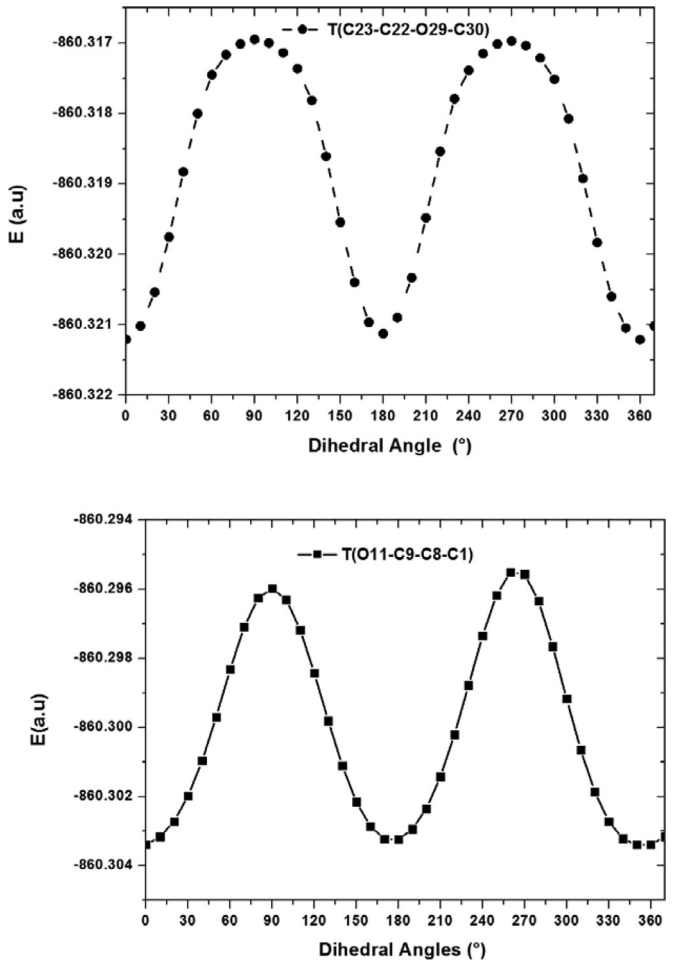

Fig. 3. Potential energy of MPAEMA molecule as a function of dihedral angle (φ).

been identified that the structure with minimum total energy of MPAEMA molecule is the C_1 form and it has been found that MPAEMA have spin singlet as the most stable (minimum total energy). Optimized geometrical parameters have been used to calculate the spectroscopic properties. In order to make the calculated vibrational frequencies more compliant with the measured results, they have been multiplied by 0.96 (above 1800 cm^{-1}) and 0.98 (under 1800 cm^{-1}) as a global scaling factor for B3LYP/6-311 + + G(d,p). The assignment of the vibrational modes has been based on calculated potential energy distributions (PEDs) using VEDA4 program [16]. ^{1}H and ^{13}C NMR isotropic chemical shifts have calculated via GIAO [17,18] with the basis set of B3LYP/6-311 + + G(d,p) in dimethyl sulfoxide (DMSO). Excitation energies have been calculated using TD-DFT method [19,20] with the 6-311 + + G(d,p) basis set [15]. TD-DFT calculations have been taken into account with solvent effects using the IEF-PCM method. It has been shown in the literature that the IEF (integral equation formalism) version of the PCM solvation model gives effective and accurate results [21]. The energy values of the highest occupied molecular orbital (E_{HOMO}) and the lowest unoccupied molecular orbital (E_{LUMO}) of the title molecule have been estimated. At the same time other electronic properties, such as chemical hardness, chemical potential, electronegativity, and electrophilicity index have been estimated [22]. The molecular electrostatic potential (MEP) and the surface map showing the molecular electron density has been evaluated and presented as 2D and 3D.

2.3. Antiproliferative effect of MPAEMA on HeLa cell line

HeLa cancer cells have used for the cytotoxicity studies. Cells have incubated in RPMI/1640 medium containing 10% FBS, and 1% gentamicin sulfate solution at 37 °C under 5% CO_2. Cytotoxic effect of MPAEMA on HeLa cells has monitored using an XTT assay (Biological Industries) according to manufacturer's instructions. Then, XTT reagent has added and absorbance of water- soluble formazan product has measured at 480 nm with 96-well plate reader (BIOTEK) after 72 h and the IC50 value has calculated.

Table 1
Geometrical parameters optimized in MPAEMA [bond length (Å) and bond angle (°)].

	Bond length		Bond length
C_1-H_2	1.070	C_9-O_{10}	1.258
C_1-H_3	1.070	C_9-O_{11}	1.430
C_1-C_8	1.355	O_{11}-C_{12}	1.430
C_4-H_5	1.070	C_{12}-H_{13}	1.070
C_4-H_6	1.070	$C_{12}-H_{14}$	1.070
C_4-H_7	1.070	$C_{12}-C_{15}$	1.540
C_4-C_8	1.540	$C_{15}-O_{16}$	1.258
C_8-C_9	1.540	$C_{15}-N_{17}$	1.470
$N_{17}-H_{18}$	1.470	$C_{20}-C_{21}$	1.401
$N_{17}-C_{19}$	1.470	$C_{20}-H_{25}$	1.070
$C_{19}-C_{20}$	1.401	$C_{21}-C_{22}$	1.401
$C_{19}-C_{24}$	1.401	$C_{21}-H_{26}$	1.070
$C_{22}-C_{23}$	1.401	$C_{22}-O_{29}$	1.430
$C_{23}-C_{24}$	1.401	$C_{23}-H_{27}$	1.070
$C_{24}-H_{28}$	1.070	$O_{29}-C_{30}$	1.430
$C_{30}-H_{31}$	1.070	$C_{30}-H_{32}$	1.070
$C_{30}-H_{33}$	1.070		
	Bond angle (°)		Bond angle (°)
$H_2-C_1-H_3$	120.0	$O_{10}-C_9-O_{11}$	120.0
$H_2-C_1-C_8$	120.0	$C_9-O_{11}-C_{12}$	109.5
$H_3-C_1-C_8$	120.0	$O_{11}-C_{12}-H_{13}$	83.6
$H_5-C_4-H_6$	109.5	$O_{11}-C_{12}-H_{14}$	82.4
$H_5-C_4-H_7$	109.5	$O_{11}-C_{12}-C_{15}$	140.4
$H_5-C_4-C_8$	109.5	$H_{13}-C_{12}-H_{14}$	138.3
$H_6-C_4-H_7$	109.5	$H_{13}-C_{12}-C_{15}$	84.3
$H_6-C_4-C_8$	109.5	$H_{14}-C_{12}-C_{15}$	81.9
$H_7-C_4-C_8$	109.5	$C_{12}-C_{15}-O_{16}$	120.0
$C_1-C_8-C_4$	120.0	$C_{12}-C_{15}-N_{17}$	120.0
$C_4-C_8-C_9$	120.0	$O_{16}-C_{15}-N_{17}$	120.0
$C_8-C_9-O_{10}$	120.0	$C_{15}-N_{17}-C_{19}$	109.5
$C_8-C_9-O_{11}$	120.0	$H_{18}-N_{17}-C_{19}$	109.5
$N_{17}-C_{19}-C_{20}$	120.0	$N_{17}-C_{19}-C_{24}$	120.0
$C_{20}-C_{19}-C_{24}$	120.0	$C_{19}-C_{20}-H_{25}$	120.0
$C_{21}-C_{20}-H_{25}$	120.0	$C_{20}-C_{21}-C_{22}$	120.0
$C_{20}-C_{21}-H_{26}$	120.0	$C_{22}-C_{21}-H_{26}$	120.0
$C_{21}-C_{22}-C_{23}$	120.0	$C_{21}-C_{22}-O_{29}$	120.0
$C_{23}-C_{22}-O_{29}$	120.0	$C_{22}-C_{23}-C_{24}$	120.0
$C_{22}-C_{23}-H_{27}$	120.0	$C_{19}-C_{24}-C_{23}$	120.0
$C_{19}-C_{24}-H_{28}$	120.0	$C_{23}-C_{24}-H_{28}$	120.0
$C_{22}-O_{29}-C_{30}$	109.5	$O_{29}-C_{30}-H_{31}$	109.5
$O_{29}-C_{30}-H_{32}$	109.5	$O_{29}-C_{30}-H_{33}$	109.5
$H_{31}-C_{30}-H_{32}$	109.5	$H_{31}-C_{30}-H_{33}$	109.5
$H_{32}-C_{30}-H_{33}$	109.5		
	Dihedral		Dihedral
$H_2-C_1-C_8-C_4$	180.0	$H_6-C_4-C_8-C_9$	90.0
$H^2-C_1-C_8-C_9$	0.0	$H_7-C_4-C_8-C_1$	30.0
$H_3-C_1-C_8-C_4$	0.0	$H_7-C_4-C_8-C_9$	−150.0
$H_3-C_1-C_8-C_9$	180.0	$C_1-C_8-C_9-O_{10}$	180.0
$H_5-C_4-C_8-C_1$	150.0	$C_1-C_8-C_9-O_{11}$	0.0
$H_5-C_4-C_8-C_9$	−30.0	$C_4-C_8-C_9-O_{10}$	0.0
$H_6-C_4-C_8-C_1$	−90.0	$C_4-C_8-C_9-O_{11}$	180.0
$C_8-C_9-O_{11}-C_{12}$	−150.0	$O_{10}-C_9-O_{11}-C_{12}$	30.0
$C_9-O_{11}-C_{12}-H_{13}$	−171.20	$C_9-O_{11}-C_{12}-H_{14}$	−30.6
$C_9-O_{11}-C_{12}-C_{15}$	−98.19	$O_{11}-C_{12}-C_{15}-0_{16}$	28.32
$O_{11}-C_{12}-C_{15}-N_{17}$	−151.67	$H_{13}-C_{12}-C_{15}-O_{16}$	101.09
$H_{13}-C_{12}-C_{15}-N_{17}$	−78.90	$H_{14}-C_{12}-C_{15}-O_{16}$	−39.41
$H_{14}-C_{12}-C_{15}-N_{17}$	140.58	$C_{12}-C_{15}-N_{17}-H_{18}$	90.0
$C_{12}-C_{15}-N_{17}-C_{19}$	−150.0	$O_{16}-C_{15}-N_{17}-H_{18}$	−90.0
$O_{16}-C_{15}-N_{17}-C_{19}$	30.0	$C_{15}-N_{17}-C_{19}-C_{20}$	−150.0
$C_{15}-N_{17}-C_{19}-C_{24}$	30.0	$H_{18}-N_{17}-C_{19}-C_{20}$	−30.0
$H_{18}-N_{17}-C_{19}-C_{24}$	150.0	$N_{17}-C_{19}-C_{20}-C_{21}$	−180.0
$N_{17}-C_{19}-C_{20}-H_{25}$	0.0	$C_{24}-C_{19}-C_{20}-C_{21}$	0.0
$C_{24}-C_{19}-C_{20}-H_{25}$	−180.0	$N_{17}-C_{19}-C_{24}-C_{23}$	180.0
$N_{17}-C_{19}-C_{24}-H_{28}$	0.0	$C_{20}-C_{19}-C_{24}-C_{23}$	−0.0
$C_{20}-C_{19}-C_{24}-H_{28}$	−180.0	$C_{19}-C_{20}-C_{21}-C_{22}$	−0.0
$C_{19}-C_{20}-C_{21}-H_{26}$	180.0	$H_{25}-C_{20}-C_{21}-C_{22}$	180.0
$H_{25}-C_{20}-C_{21}-H_{26}$	−0.0	$C_{20}-C_{21}-C_{22}-C_{23}$	−0.0
$C_{20}-C_{21}-C^{22}-O29$	180.0	$H_{26}-C_{21}-C_{22}-C_{23}$	180.0

(*continued on next page*)

Table 1 (*continued*)

	Bond length		Bond length
$H_{26}-C_{21}-C_{22}-O_{29}$	−0.0	$C_{21}-C_{22}-C_{23}-C_{24}$	0.0
$C_{21}-C_{22}-C_{23}-H_{27}$	−180.0	$O_{29}-C_{22}-C_{23}-C_{24}$	−180.0
$O_{29}-C_{22}-C_{23}-H_{27}$	0.0	$C_{21}-C_{22}-O_{29}-C_{30}$	−30.0
$C_{23}-C_{22}-O_{29}-C_{30}$	150.0	$C_{22}-C_{23}-C_{24}-O_{19}$	−0.0
$C_{22}-C_{23}-C_{24}-H_{28}$	180.0	$H_{27}-C_{23}-C_{24}-H_{28}$	−0.0
$C_{22}-O_{29}-C_{30}-H_{31}$	60.0	$C_{22}-O_{29}-C_{30}-H_{32}$	−60.0
$C_{22}-O_{29}-C_{30}-H_{33}$	−180.0		

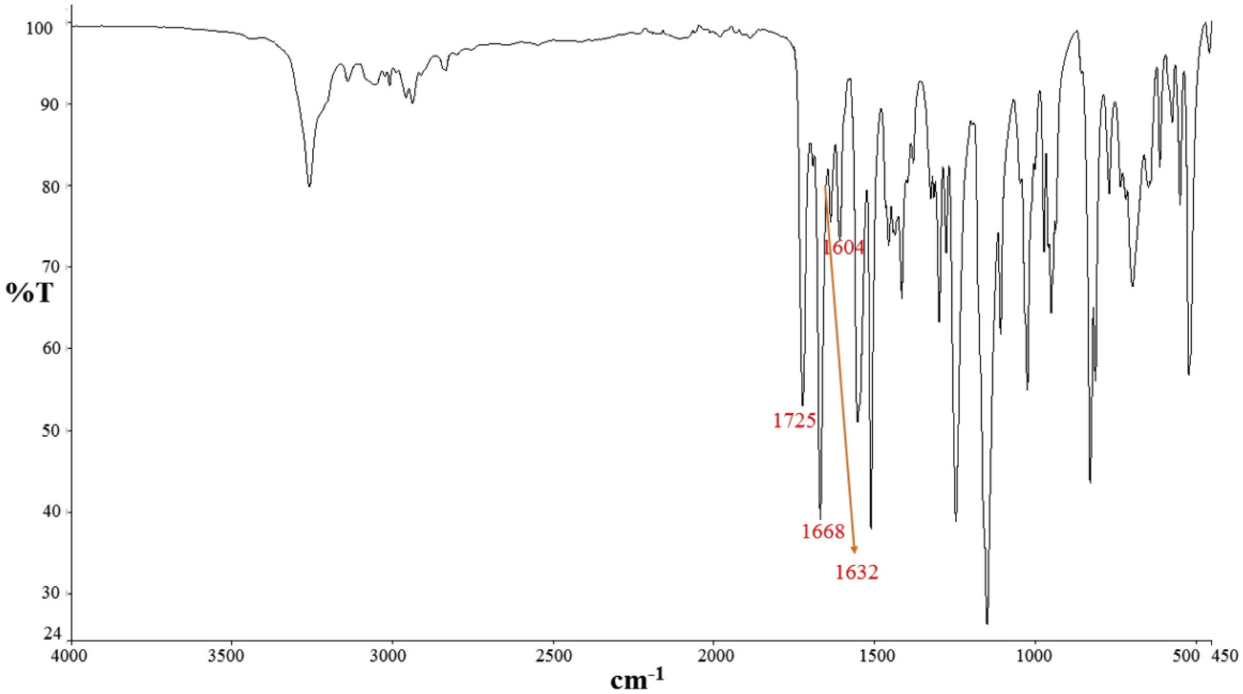

Fig. 4. The experimental FTIR spectrum of MPAEMA.

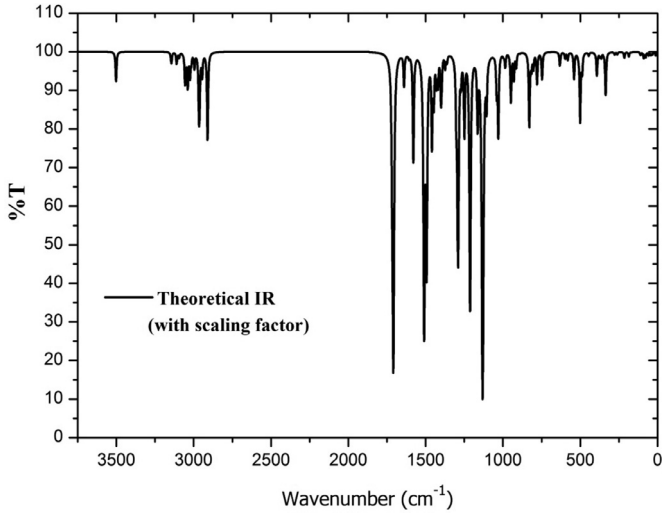

Fig. 5. The calculated (with the scale factor) FTIR spectrum of MPAEMA.

Table 2
Comparison of the calculated and experimental vibrational spectra and proposal assignments of MPAEMA.

No	Experimental wavenumber FTIR	Theoretical wavenumber Scaled	PED(%10) Assignments
1		11	ΓCNCC(12), ΓOCCN(74)
2		27	ΓCNCC(24), ΓCOCC(22), ΓCCNC(24), ΓNCCC(11)
3		33	ΓCCOC(40), ΓCCCO(25)
4		43	ΓCNCC(40), ΓCCCO(20), ΓOCCN(15)
5		57	ΓCCOC(23), ΓCCCO(17), ΓCCNC(12)
6		77	ΓCOCC(37), ΓCCCO(28)
7		90	ΓCOCC(60), ΓCCNC(12)
8		111	δCNC(28), δNCC(23), δCCN(23), ΓCCOC(10)
9		167	ΓHCCC(14), ΓCCCC(17), ΓCCNC(13)
10		168	ΓHCCC(46), ΓCCCC(13), ΓCCNC(11)
11		187	δCCO(34), δCCC(17)
12		216	δOCC(25), δCOC(25)
13		240	ΓHCOC(72)
14		262	δCOC(10), δCCC(13), δCCN(19)
15		280	γOCC(26), γCCN(10)
16		339	γOCO(21), γCOC(26), γCCC(27)
17		353	γOCN(20), γCNC(10), γCNC(25), δCOC(14)
18		368	δCCC(10), ΓCCCC(17), ΓOCCC(18), ΓNCCC(17)
19		377	δCCC(21), ΓCCCC(24)
20		396	δCCC(12), ΓCCCC(24)
21		413	ΓHCCC(33), ΓCCCC(62)
22		450	δCCC (18), δOCC(19), δCOC(15)
23		492	δCCO(21), δCCC(11), ΓHNCC(11)
24		506	δCOC(34)
25		518	ΓHNCC(21), ΓOCCC(22), ΓNCCC(23)
26		546	δCOC(12), ΓHNCC(14)
27		587	ΓHNCC(11), ΓOCNC(35)
28		604	νCC(29), δOCO(25)
29		635	δCCC(37)
30		639	ΓHCCC(96), ΓOCOC(21)
31		711	ΓCCCC(58), ΓOCCC(11)
32		741	νOC(10), δCCC(11), δOCC(16)
33		755	νOC(11), ν(CC(18), δOCN(13), δCCC(12)
34		788	ΓHCCC(78)
35		812	νOC(14), ΓOCOC(22)
36	814	824	ΓOCOC(30), ΓCCCC(10)
37		838	ΓHCCC(65), ΓOCCC(12)
38	830	839	ν (CC(13), δCCC(21)
39		899	ΓHCCC(84)
40		924	ν (46), δHCC(25)
41		939	νCC(30), δOCN(16), δCNC(11)
42		958	ΓHCCC(95)
43	950	965	ΓHCCC(80), ΓCCCC(12)
44	974	995	δHCC(24), ΓHCCC(19)
45		1003	δCCC(74)
46		1007	ΓHCOC(26), ΓCOCC(14), ΓOCNC(16)
47	1025	1041	νOC(70)
48		1050	γHCH(25), Γ HCCC(48)
49		1052	νOC(46)
50	1108	1117	νCC(22), γHCC(44)
51		1143	νOC(40), γOCO(10)
52		1146	γHCH(28), ΓHCOC(72)
53		1175	γHCC(48)
54		1176	νNC(17)
55		1179	γHCH(13), ΓHCOC(46)
56		1226	νCC(12), νOC(13), νNC(21)
57	1247	1262	νCC(13), νOC(28), νNC(13)
58	1277	1285	γHCO(67)
59		1303	γHCC(21)
60		1307	νCC(10), γHCC(36)
61	1298	1315	νCC(34)
62		1376	γHCH(15), ΓHCOC(58)
63		1388	γHCH(74)
64		1411	γHCH(79)
65		1415	νCC(34), δHCC (12)
66	1416	1435	δHCH (80), ΓHCOC(14)
67		1444	δHCH(82), ΓHCOC(11)

(*continued on next page*)

Table 2 (*continued*)

No	Experimental wavenumber FTIR	Theoretical wavenumber Scaled	PED(%10) Assignments
68		1447	δHCH(100)
69		1462	δHCH(70), ΓHCCC(21)
70		1463	δHCH(76), ΓHCOC(16))
71		1475	δHCH(78), ΓHCOC(20)
72		1510	δHCC(55), δCCC(10)
73	1512	1526	νNC(12), δHNC(44)
74	1550	1596	νCC(38), δHNC(12), δCCC(13)
75	1604	1624	νCC(65)
76	1632	1657	νCC(70), δHCH(12)
77	1668	1727	νOC(83)
78	1725	1734	νOC(83)
79	2900	2880	νCH(92)
80	2940	2915	νCH(100)
81		2931	νCH(100)
82		2935	νCH(100)
83		2965	νCH(100)
84		2985	νCH(100)
85		2992	νCH100)
86		3007	νCH(92)
87		3021	νCH(99)
88		3025	νCH(97)
89		3062	νCH(98)
90		3078	νCH(97)
91		3111	νCH (98))
92	3259	3114	νCH(100)
93	3300	3466	νNH(100)

υ, stretching; δ, in plane bending; γ, out of plane bending; Γ, torsion; ρ, scissoring.

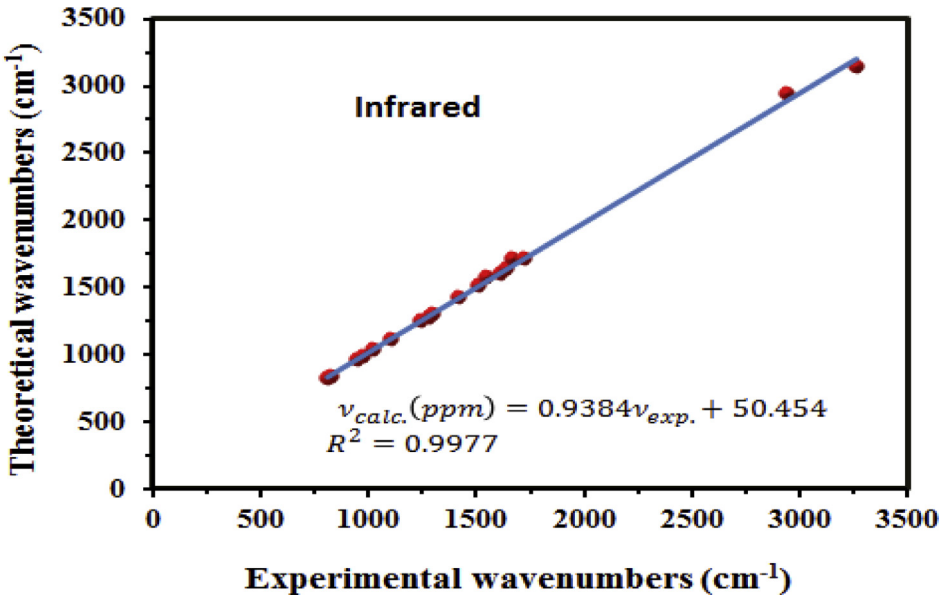

Fig. 6. Correlation graphic of calculated and experimental frequencies MPAEMA.

3. Results and discussion

3.1. Characterization of MPAEMA

The calculated geometrical parameters of the MPAEMA at the B3LYP/6-311 + + (d,p) level of theory are listed (Table 1).

Vibrational modes, ^{1}H and ^{13}C NMR chemical shifts and HOMO-LUMO molecular orbital calculations have found with the same level of DFT method. FTIR spectrum has recorded with Perkin Elmer Spectrum Two (UATR) IR spectrophotometer. The molecule has a C_1 symmetry and 93 modes of fundamental vibration. Measured and calculated IR spectrum of the molecule is presented in Figs. 4

Table 3
Experimental and calculated chemical shifts (ppm) for MPAEMA.

Atom	B3LYP/6-311G ± +(d.p) DMSO	Experimental DMSO
15-C	215	166
9-C	186	165
22-C	161	155
8-C	144	135
19-C	143	132
1-C	137	127
24-C	124	121
20-C	117	121
23-C	115	114
21-C	114	114
12-C	69	63
30-C	53	55
4-C	18	18
14-H	12.60	4.6
13-H	8.50	4.6
26-H	7.74	6.7
28-H	7.59	7.3
27-H	6.99	6.7
25-H	6.95	7.3
2-H	6.54	5.9
3-H	6.44	5.6
18-H	5.68	7.3
31-H	4.20	3.6
33-H	3.32	3.6
32-H	2.57	3.6
6-H	1.77	1.8
5-H	1.68	1.8
7-H	1.55	1.8

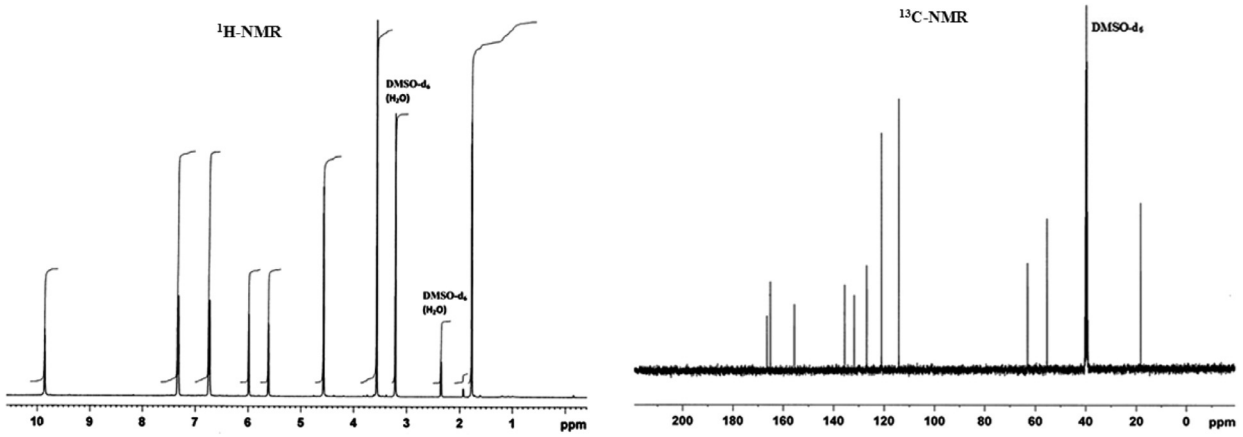

Fig. 7. ^{1}H NMR and ^{13}C NMR spectra of MPAEMA in DMSO solution.

and 5, respectively. At the same time, theoretical wavenumbers and the potential energy distributions of the vibrational modes for headline molecule are listed in Table 2, in comparison with the observed vibrational spectra of this molecule.

The most characteristic peaks observed in FTIR are as follows: C—C aromatic stretch peak visible at 1100–1650 cm^{-1} with not being significantly affected by the circumference [23] this stretch bond has been observed 1604 cm^{-1} and calculated at 1624 cm^{-1}. C═C olefinic stretch recorded at 1637 cm^{-1} in previous study [24], the peak of C═C olefinic stretching vibration observed at 1632 cm^{-1}, theoretical scaled frequencies have been calculated at 1657 cm^{-1}. The PED contributions are 70%. C O amide stretch has been observed as 1668 cm^{-1} and calculated as 1727 cm^{-1}. C═O stretching vibration has been observed in the range of 1850–1550 cm^{-1} [25]. In this study, this vibration band has been recorded at 1725 cm^{-1}. The calculated scaled frequencies are 1734, 1727 cm^{-1} and its contribution of PED is 83%. N—H aromatic stretch appears at 3390 + −60 cm^{-1} [26]. N—H stretching frequency has been observed as 3300 cm^{-1} and calculated as 3466 cm^{-1}. The contribution of PED of N—H band is 100%. C—H aliphatic stretch has been observed in the region 3107–2935 cm^{-1} in previous study [24]. In the present study, the peak C—H aliphatic stretching vibration is observed at 2900 cm^{-1}. These modes have been calculated as 3021–2880 cm^{-1} with B3LYP/6-311 + +G(d,p) level, respectively. The other modes can also be seen from Table 2. The results are principally in accordance with each other,

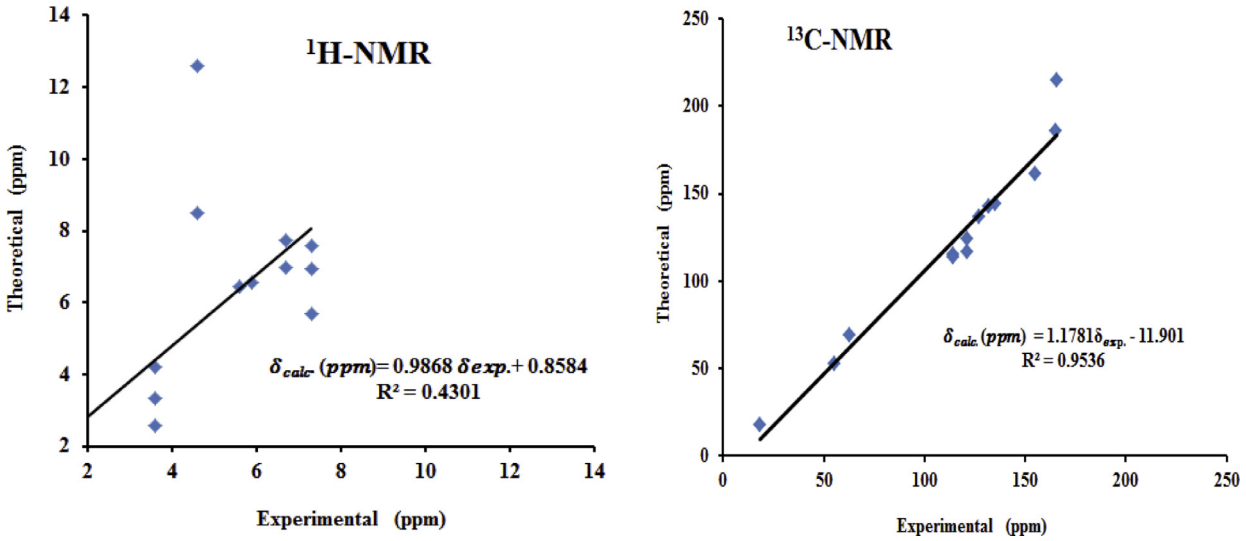

Fig. 8. Correlation graphic of calculated and experimental (total) chemical shifts of MPAEMA.

Table 4
Comparison of experimental (in ethanol, DMSO, water and gas solutions) and calculated absorption wavelength (λ, nm), excitation Energies (E, eV) and oscillator strength (*f*) of MPAEMA.

TD-DFT/ B3LYP/6-311 + +G(d,p) (Theoretical)					Experimental		
λ (nm)	E (eV)	*f*	Assignments Chloroform	Major contributions	Chloroform λ (nm)	E(eV)	*f*
502	1.1497	0.0014	π–π*	H→L, H−1→L, H→L + 1	230	0.0864	0.0130
250	2.4670	0.0744	π–π*				
146	2.5015	0.0737	π–π*	H→L + 1			

albeit some differences. Those differences may result from the effects that free molecules in the gas phase have been used for calculations, although solid sample has been performed for measurement. The correlation between the experimental and theoretical vibrational modes has been presented in Fig. 6.

NMR spectra have been obtained on a Bruker 400 MHz spectrometer in DMSO-d_6 and have been calculated in DMSO solvent by using The Gauge Independent Atomic Orbital (GIAO) method at B3LYP/6-311 + +G(d,p) level of theory, as depicted in Table 3. Tetramethylsilane (TMS) has been considered internal reference. Theoretically calculated ^{13}C NMR shifts have been compared to experimental data before they have been scaled with the equation $\delta_{scal} = 0.95\delta_{calc} + 0.30$ [27].

The experimental ^{1}H and ^{13}C NMR spectra of the molecule have been taken in DMSO and have been presented respectively in Fig. 7. Correlation graphics between the observed and calculated chemical shifts have been drawn in Fig. 8. The square root correlation factor (R^2) for ^{13}C have been calculated to be 0.9536 and 0.4301 for ^{1}H. The isotropic chemical shifts have been used in the identification of ionic species and reactive organic. Experimental shifts of the solvent prepared in DMSO-d_6 is observed as follow: ^{1}H NMR spectrum; NH structure at 9.9 ppm, ring protons at 7.3, 6.7 ppm, O−CH_2 protons at 4.6 ppm, CH_2 olefinic protons at 5.9, 5.6 ppm, O−CH_3 proton at 3.6 ppm, C−CH_3 proton at 1.8 ppm. The theoretical shifts of the solvent prepared in DMSO solvent. Chemical shifts protons of the title compound have been calculated in the ranges 1.8–7.3 ppm. Except for 13H, 14H and 18H atoms, it seems that there is generally agreement between experimental and theoretical results. These atoms have been affected by electronegative atoms such as oxygen and nitrogen in their surroundings and showed a higher shift in ppm. Also, Equivalent and singlet peak values for 31, 32 and 33-H protons in the NMR has been an expected outcome, despite the theoretically different ppm value expectations for the above mentioned atoms being affected from the electronegative O-29. Similarly, 5-H, 6-H and 7-H atoms giving a singlet peak value equivalent to 3 protons, and 13-H and 14-H atoms giving a singlet peak value equivalent to 2 protons is an expected outcome. 2-H and 3-H atoms, being affected from the surrounding protons have formed a double doublet at 5.6 and 5.9 ppm.

^{13}C NMR spectrum for the title molecule, C═O amide carbon at 166 ppm, C══O ester carbon at 165 ppm, ring carbons at 155, 132, 121, 114 ppm, CH_3−C═at 135 ppm, = CH olefinic carbon at 127 ppm, O═C−CH_2−O structure at 63 ppm, O−CH_3 structure at 55 ppm, and the C−CH_3 structure peaked at 18 ppm. The calculated carbon NMR chemical shifts have been obtained in the ranges at 18–215 ppm. Looking at the theoretical calculated values and experimental data at Table 3, C═O amide carbon atom (15-C) gets affected from the surrounding electronegative N and O atoms, and gives the highest ppm peak value. Similarly, C═O ester carbon (9-C) gets affected from the surrounding O atoms and gives a peak value at high ppm. Although there is no electronegative atom bonded

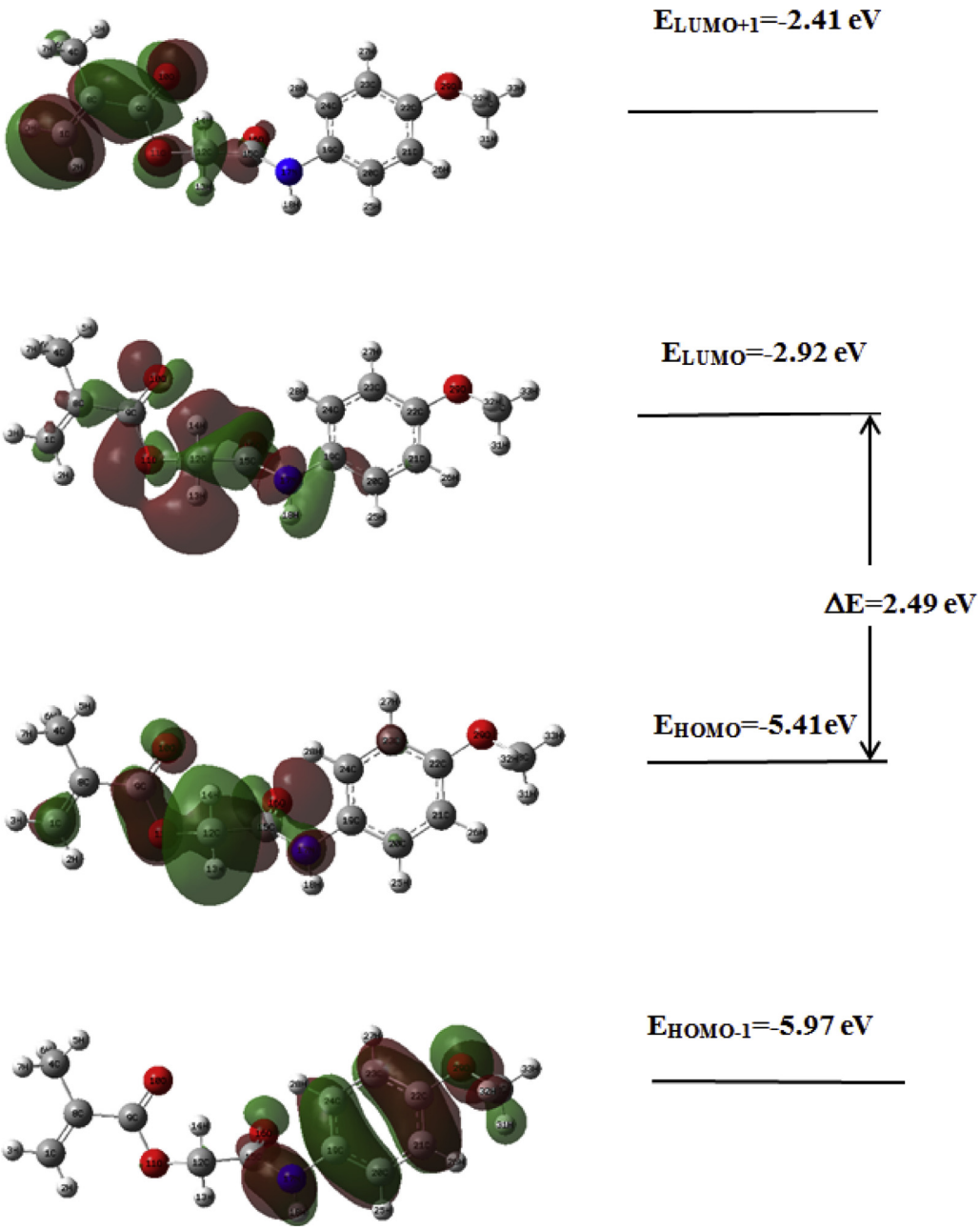

Fig. 9. The frontier molecular orbitals of MPAEMA for gas phase.

to the 12-C atom, it gets affected from the surrounding electronegative atoms.

3.2. UV−Vis analysis

The changes in the electronic states of the title molecule have been computed with TD-DFT-B3LYP/6-311 + + G(d,p) basis set in chloroform. The theoretical and measured excitation energies, UV−Vis absorption spectrum and electronic parameters of molecule are given in Table 4. Absorption spectrum for MPAEMA has been calculated at 146, 250, 502 nm, observed electronic transition showed one band at 230 nm in chloroform solution.

3.3. Frontier molecular orbitals analysis

The plots of the HOMOs and LUMOs are seen in Fig. 9 for gas phase. While HOMO energy is directly associated with the ionization

Table 5
The calculated energies values of MPAEMA molecules using by the TD-DFT/B3LYP method using 6-311G + + (d,p) basis set.

	Gas	DMSO	Water	Chloroform
E_{total} (Hartree)	−859.97229969	−859.99262545	−859.99296485	−859.98630131
E_{HOMO} (eV)	−5.41	−5.71	−5.71	−5.61
E_{LUMO} (eV)	−2.92	−3.07	−3.07	−3.02
E_{HOMO-1} (eV)	−5.97	−6.22	−6.22	−6.13
E_{LUMO+1} (eV)	−2.41	−2.42	−2.42	−2.41
$E_{HOMO-1–LUMO+1\ gap}$ (eV)	−3.56	−3.80	−3.80	−3.73
$E_{HOMO–LUMO\ gap}$ (eV)	−2.49	−2.64	−2.64	−2.59
Chemical hardness (h)	−1.25	−1.32	−1.32	−1.30
Electronegativity (χ)	4.16	4.39	4.39	4.31
Chemical potential (μ)	−4.16	−4.39	−4.39	−4.31
Electrophilicity index (ω)	−6.95	−7.29	−7.30	−7.30

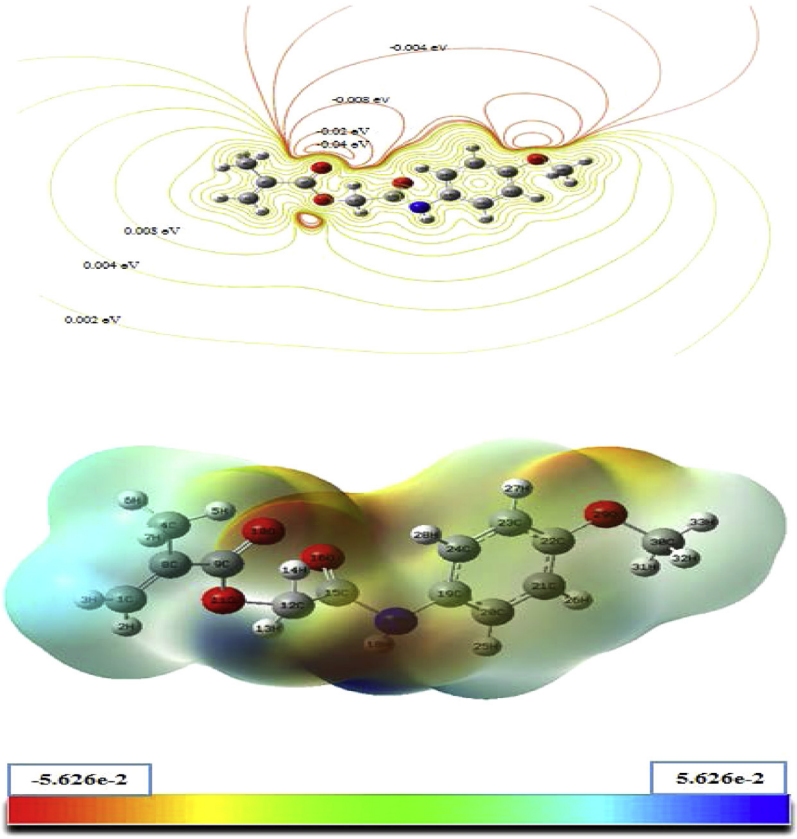

Fig. 10. Molecular electrostatic potential (MEPs) map for MPAEMA molecule.

potential (I), energy of the LUMO is directly associated with the electron affinity (A) [28,29]. In addition, MO theory, which is often used by chemist is important in terms of describing terms such as chemical potential (μ), ionization potential (I), electronegativity (χ), electron affinity (A), electrophilicity index (w), hardness (η) and softness (S). By Koopman [30] for closed shell components η, μ, and χ can be defined as η = I-A, μ = (I-A)/2, χ = (I + A)/2. Electron affinity and ionization potential can be estimated through HOMO and LUMO orbital energies as A = − E_{LUMO} and I = − E_{HOMO}. The electronegativity and hardness are used generally to make predictions almost chemical reactivity. Also, if a molecule has small frontier orbital gap, it is called a soft molecule and is more polarizable and has a high chemical reactivity as well as low kinetic stability [31]. Fully optimized ground state structures of title molecule have been used at TD-DFT/B3LYP/6–311 + + G(d,p) level to find the energies (Table 5) and plots (Fig. 9) of HOMO (MO 46), LUMO (MO 47), HOMO-1 (MO 45) and LUMO + 1 (MO 48) of MPAEMA molecule.

These molecular orbitals related to electronic transitions have been calculated in DMSO, water, and chloroform solvents and in gas phase (Table 4). It is known that if reactivity of a molecule is high, the value of the energy gap is small. In this study, energy gap of title molecule have been found to be same value (2.64 eV) for DMSO and water solutions and different value (2.49 eV, 2.59 eV) for the chloroform and gas phase. This can be explained by MPAEMA molecule having more reactivity in gas phase. Likewise, chemical

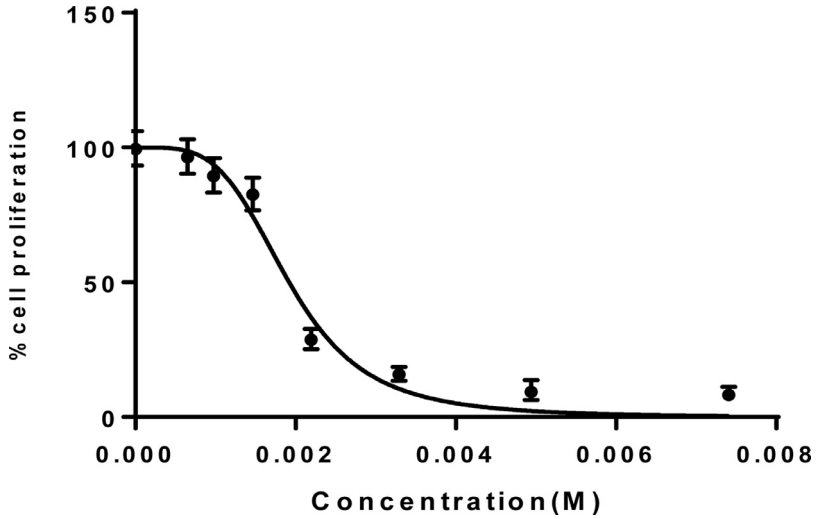

Fig. 11. Cytotoxicity analyses of MPAEMA on HeLa cells.

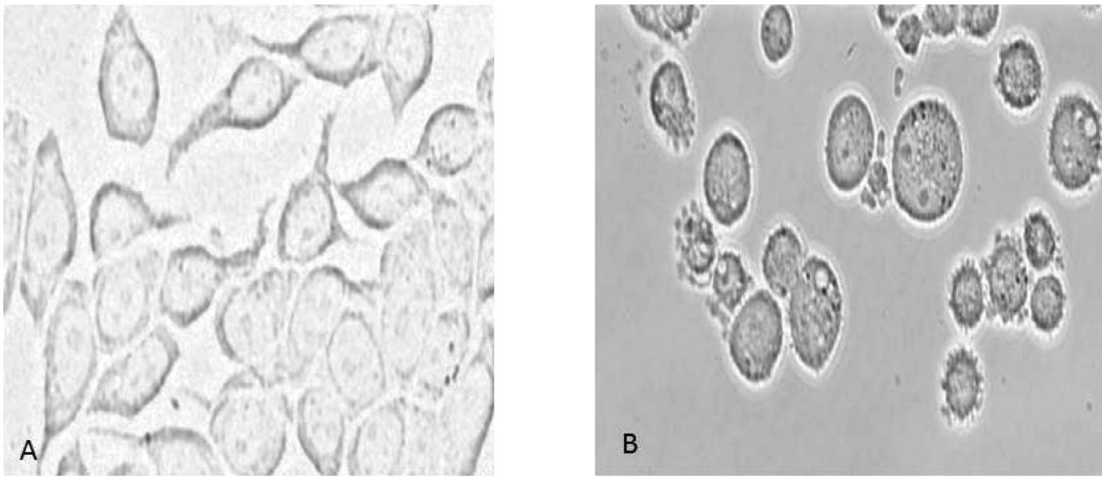

Fig. 12. Effect of MPAEMA on cells by inverted light scattering microscopy (A) non-treated cells (control), (B) cells treated with MPAEMA.

hardness is inversely proportional to reactivity. Therefore, a molecule with a small energy gap value is softer and is more reactive. In this work, the chemical hardness value of MPAEMA is the lowest in the gas phase and has a value of 1.25 eV.

3.4. Molecular electrostatic potential (MEP) analysis

In order to estimate electrophilic and nucleophilic reactive location for the title compound, MEP has been calculated by using optimized structure at B3LYP/6-311 + + G(d,p) level. In our study, MEP-3D plots and contour map (2D contour) for MPAEMA are illustrated in Fig. 10. The meaning of the color scheme on the MEP surface is as follows: red color represents electronically rich region, while partly negative charge is represented by blue color for electron-deficient region, partly positive charge is represented by light blue color for lightly electron deficient region, yellow color is used for lightly electron rich region, and green color is used for neutral. In this study, the color coding is in the range between − 0.0562 a.u. (dark red) and 0.0562 a.u. (dark blue) in molecule. As seen from the MEPs, while the region near the CH groups have positive potential, the regions over the oxygen atoms have negative potential for MPAEMA.

4. Antiproliferative activity on HeLa cell line

Cell proliferation assay has been performed by using XTT reagent to determine the effects of MPAEMA on HeLa cells. XTT results demonstrate the antiproliferative effect of MPAEMA on HeLa cells. The determined IC50 value for HeLa cells is 1.8 mM by MPAEMA (Figs. 11 and 12). Ernawati et al. [32] showed that IC50 values of methyl 3-(4-nitrophenyl) acrylate and methyl 3-(2- nitrophenyl) acrylate found on Murine Leukemia cell lines 7.98 μg/mL, 27.78 μg/mL respectively. We demonstrated that MPAEMA is new

synthesized molecule. And functional groups of molecule may be masked, closing positions etc., so it may not show toxic effect. In addition methyl acrylate is used commonly in the synthesis of drug loaded nanoparticles such as dendrimer to treat cancer [33,34]. In the light of this information, this newly synthesized molecule can be used in drug development because of its low toxic effect.

5. Conclusion

In this study, synthesized 2-(4-methoxyphenylamino) – 2-oxoethyl methacrylate (MPAEMA) compound has been obtained with the 2-stage reaction and characterized by FTIR, ^{1}H and ^{13}C-NMR spectroscopy techniques. Both experimental and theoretical methods have shown that the compound has been successfully synthesized. The results have shown that the calculated frequencies corresponded to the experimental values except for some deviations. We think that the deviations between these experimental and theoretical results are due to the fact that theoretical calculations are made in gas phase and for a single molecule, and experimental results are made in the presence of intermolecular interactions. The fundamental vibrations of the title molecule has been assigned by means potential energy distributions (PEDs) using VEDA4 program. HOMO, LUMO energies and other related molecular properties have been calculated to have more information about the molecule. The HOMO-LUMO energy gap is the same in DMSO and water solubility, with different values in chloroform solvent and gas phase. The HOMO-LUMO low energy gap and other reactivity identifiers in all solvents of the molecule showed that the molecule has a bioactive property. Furthermore, antiproliferative effect of MPAEMA on HeLa cell line has been determined in this study. HeLa cells have been initially isolated from a highly aggressive cervical cancer. The obtained results in HeLa cells indicated that MPAEMA has antitumor activity with low toxicity. On the other hand, IC50 value for MPAEMA against different cancer cells and normal cells may be very high. Low toxicity of this molecule may be due to various mechanism such as, its low solubility, effective biotransformation, molecular pathways. The obtained results in HeLa cells indicated that MPAEMA is safe compound and appropriate for therapeutic use.

References

[1] G. Barim, M.G. Yayla, M. Degirmenci, Copolymerization of cyclohexene-3-yl methyl methacrylate with styrene: synthesis, characterization, monomer reactivity ratios, and thermal properties, Des. Monomers Polym. 17 (2014) 610–616.
[2] J.W. Nicholson, P.J. Brookman, O.M. Lacy, G.S. Sayers, A.D. Wilson, A study of the nature and formation of zinc polyacrylate cement using fourier transform infrared spectroscopy, J. Biomed. Mater. Res. 22 (1988) 623–631.
[3] S. Parker, M. Braden, Water absorption of methacrylate soft lining materials, Biomaterials 10 (1989) 91–95.
[4] J.N. Patel, M.B. Dolia, K.H. Patel, R.M. Patel, Homopolymer of 4-chloro-3-methyl phenyl methacrylate and its copolymers with butyl methacrylate: synthesis, characterization, reactivity ratios and antimicrobial activity, J. Polym. Res. 13 (2006) 219–228.
[5] J.S. Al–Otaibi, R.I. Al–Wabli, Vibrational spectroscopic investigation (FT-IR and FT-Raman) using ab initio (HF) and DFT (B3LYP) calculations of 3-ethoxymethyl-1,4-dihydroquinolin-4-one, Spectrochim. Acta Part A 137 (2015) 7–15.
[6] R.A. Friesner, R.B. Murphy, M.D. Beachy, M.N. Ringnalda, W.T. Pollard, B.D. Dunietz, Y. Cao, Correlated ab initio electronic structure calculations for large molecules, J. Phys. Chem. A 103 (1999) 1913–1928.
[7] T. Ziegler, Approximate density functional theory as a practical tool in molecular energetics and dynamics, Chem. Rev. 91 (1991) 651–667.
[8] F. Bezgin, N. Ayaz, K. Demirelli, Synthesis, characterization, and dielectric properties of polymers functionalized with coumarone and diethanolamine, J. Appl. Polym. Sci. 132 (2015) 42164–42174.
[9] N. Çankaya, G. Besci, Synthesis, characterization, thermal properties and reactivity ratios of methacrylate copolymers including methoxy group, J. Fac. Eng. Archit. Gazi Uni. 2018 (2018) 1–24.
[10] Y. Açıkbaş, N. Çankaya, R. Capan, M. Erdogan, C. Soykan, Swelling behavior of the 2-(4-methoxyphenylamino)-2-oxoethyl methacrylate monomer LB thin film exposed to various organic vapors by quartz crystal microbalance technique, J. Macromol. Sci. Part A 53 (2016) 18–25.
[11] T. Daşbaşı, Ş. Saçmacı, N. Çankaya, C. Soykan, A new synthesis, characterization and application chelating resin for determination of some trace metals in honey samples by FAAS, Food Chem. 203 (2016) 283–291.
[12] A.D. Becke, Density-functional exchange-energy approximation with correct asymptotic behavior, Phys. Rev. A 38 (1998) 3098–3100.
[13] C. Lee, W. Yang, R.G. Parr, Development of the Colle-Salvetti correlation-energy formula into a functional of the electron density, Phys. Rev. B 37 (1988) 785–789.
[14] P.C. Hariharan, J.A. Pople, The influence of polarization functions on molecular orbital hydrogenation energies, Theor. Chim. Acta. 28 (1973) 213–222.
[15] M.J. Frisch, GAUSSIAN 09, Revision A.1, Gaussian Inc., Wallingford, CT, 2009.
[16] M.H. Jamroz, Vibrational energy distribution analysis (VEDA): scopes and limitations, Spectrochim. Acta Part A 114 (2013) 220–230.
[17] R. Ditchfield, Molecular orbital theory of magnetic shielding and magnetic susceptibility, J. Chem. Phys. 56 (1972) 5688–5691.
[18] K. Wolinski, J.F. Hinton, P. Pulay, Efficient implementation of the gauge-independent atomic orbital method for NMR chemical shift calculations, J. Am. Chem. Soc. 112 (1990) 8251–8260.
[19] M. Marques, E. Gross, Time-dependent density functional theory, Annu. Rev. Phys. Chem. 55 (2004) 427–455.
[20] F. Furche, K. Burke, Time-dependent density functional theoryin quantum chemistry, Ann. Rep. Comput. Chem. 1 (2005) 19–30.
[21] J. Tomasi, B. Mennucci, E. Cancès, The IEF version of the PCM solvation method: an overview of a new method addressed to study molecular solutes at the QM ab initio level, J. Mol. Str. (Theochem) 464 (1999) 211–226.
[22] C.G. Zhan, J.A. Nichols, D.A. Dixon, Ionization potential, electron affinity, electronegativity, hardness, and electron excitation energy: molecular properties from density functional theory orbital energies, J. Phys. Chem. A. 107 (2003) 4184–4195.
[23] N. Sundaraganesan, S. Illakiamani, C. Meganathan, B.D. Joshua, Vibrational spectroscopy investigation using ab initio and density functional theory analysis on the structure of 3-aminobenzotrifluoride, Spectrochim. Acta A 67 (2007) 214–224.
[24] F. Akman, Experimental and theoretical investigation of molecular structure, vibrational analysis, chemical reactivity, electrostatic potential of benzyl methacrylate monomer and homopolymer, Can. J. Phys. 94 (2016) 1–12.
[25] G. Socrates, Infrared and Raman Characteristics Group Frequencies, Tables and Charts, third ed., Wiley, Chichester, 2001.
[26] C.S. Abraham, J.C. Prasana, S. Muthu, Quantum mechanical, spectroscopic and docking studies of 2-Amino-3-bromo-5-nitropyridine by density functional method, Spectrochim. Acta Part A 181 (2017) 153–163.
[27] A.E. Aliev, D. Courtier-Murias, S. Zhou, Scaling factors for carbon NMR chemical shifts obtained from DFT B3LYP calculations, J. Mol. Struct. Theochem. 893 (2009) 1–5.
[28] V.K. Shukla, E.S. Al-Abdullah, A.A. El- Emam, A.K. Sachan, S.K. Pathak, A. Kumar, O. Prasad, A. Bishnoi, L. Sinha, Spectroscopic (FT-IR, FT-Raman, and UV–visible) and quantum chemical studies on molecular geometry, Frontier molecular orbitals, NBO, NLO and thermodynamic properties of 1-acetylindole, Spectrochim. Acta Part A 133 (2014) 626–638.
[29] D. Shoba, S. Periandi, S. Boomadevi, S. Ramalingam, E. Fereyduni, FT-IR, FT-Raman, UV, NMR spectra, molecular structure, ESP, NBO and HOMO–LUMO

investigation of 2-methylpyridine 1-oxide: A combined experimental and DFT study, Spectrochim. Acta Part A 118 (2014) 438–447.
[30] T. Koopmans, About the assignment of wave functions and eigenvalues to the individual electrons of an atom, Physica 1 (1934) 104–113.
[31] R.S. Mulliken, A new electroaffinity scale; together with data on valence states and on valence ionization potentials and electron affinities, J. Chem. Phys. 2 (1934) 782–793.
[32] T. Ernawati, Z. Khoirunni'mah, Synthesis methyl nitrophenyl acrylate and cytotoxic activity test against P388 leukemia cells, Indones. J. Chem. 15 (2015) 70–76.
[33] A. Zarebkohan, F. Najafi, H.R. Moghimi, M. Hemmati, M.R. Deevband, B. Kazemi, Synthesis and characterization of a PAMAM dendrimer nanocarrier functionalized by SRL peptide for targeted gene delivery to the brain, Eur J Pharm Sci. 78 (2015) 19–30.
[34] K. Owczarek, O. Nowacka, B. Klajnert, J. Kujawa, M. Bryszewska, Interaction between polyamidoamine (PAMAM) dendrimers and bovine insülin, Neuro Endocrinol. Lett. 34 (2013) 573–578.